Journal of Alloys and Compounds 513 (2012) 573–579

Contents lists available at SciVerse ScienceDirect

Journal of Alloys and Compounds

journal homepage: www.elsevier.com/locate/jallcom

Effects of multi-element dopants of TiO_2 for high performance in dye-sensitized solar cells

Ji Sun Im, Jumi Yun, Sung Kyu Lee, Young-Seak Lee*

Department of Fine Chemical Engineering and Applied Chemistry, BK21-E²M, Chungnam National University, Daejeon 305-764, Republic of Korea

ARTICLE INFO

Article history:
Received 6 August 2011
Received in revised form 29 October 2011
Accepted 2 November 2011
Available online 9 November 2011

Keywords:
Electrode materials
Semiconductors
Electrochemical reactions
Electrochemical impedance spectroscopy

ABSTRACT

Multi-inorganic element-doped TiO_2 was prepared as a semiconductor in the working electrode of a dye-sensitized solar cell (DSSC). The particle size of TiO_2 decreased by about 20% after the use of a paint shaker that enlarged the contact area between the TiO_2 and the dye or electrolyte. The fill factor and efficiency of the DSSC improved by around 14% and more than a factor of 3, respectively, based on the effects of multi-element dopants and the size reduction of TiO_2. The mechanism was suggested by electrochemical impedance spectroscopy, intensity-modulated photocurrent spectroscopy, and intensity-modulated photovoltage spectroscopy analysis methods. It seems that the doped multi-inorganic elements (B, C, N and F) prevent the electrons in the conduction band of TiO_2 from returning to the dye or electrolyte for recombination by improved electron transfer. In addition, the reduced size of TiO_2 was beneficial for active reactions at the TiO_2/dye/electrolyte interface by enlarging the contact area.

1. Introduction

The dye-sensitized solar cell (DSSC) has attracted attention as an alternative energy device for dealing with fossil energy depletion because it has many advantages such as low cost, a simple manufacturing process, low environmental loads and high efficiency in converting solar energy into electricity [1–3]. However, the industrialization of DSSCs suffers from insufficient efficiency. Therefore, numerous studies to improve the efficiency of DSSCs have been presented. They can be categorized into four types: (1) efficient dyes for high sensitivity of the solar cell, (2) working electrode system development for easy charge transfer through the conduction band of the semiconductor, (3) electrolytes with efficient redox couples such as iodide ions and tri-iodide ions and (4) counter electrode systems for maximized electron transport [4–6].

Among these approaches, the efficiency of the working electrode system was investigated in this study because the major lack for high performance DSSC is low efficient electron transfer in working electrode. In the working electrode system, the electrons excited in the lowest unoccupied molecule orbital (LUMO) of the dye are transferred to the conduction band (CB) of TiO_2 and then travel to the FTO glass. In this process, a lot of electrons in the CB of TiO_2 travel to the dye or electrolyte by trapping–detrapping events before reaching the FTO glass collecting electrode. This phenomenon results in the low efficiency of the DSSC [7–9]. Therefore, investigations on preventing the electron trapping effects in the CB of TiO_2 have been carried out by many researchers.

In this study, the inorganic element doping method was used to obtain a high efficiency of the DSSC by preventing the electron trapping effects in the CB of TiO_2. The relation between DSSC efficiency and multi-element dopants was investigated based on efficient electron transfer in the CB of TiO_2. In addition, the size reduction effects were observed to lead to an enlarged contact area of TiO_2 with the dye or electrolyte, and these effects were further investigated. The mechanism of improved efficiency of DSSCs was also investigated by electrochemical analysis based on inorganic element dopants and size reduction of TiO_2.

2. Materials and methods

2.1. Preparation of multi-inorganic-element-doped TiO_2

Commercial TiO_2 (anatase, 99.7%, 5 g, Aldrich) and tetraethylammonium tetrafluoroborate ($(CH_3CH_2)_4N^+BF_4^-$, TEATFB, 99%, 2.17 g, 0.01 M, Mw: 217 g, Aldrich) were mixed with distilled water (25 ml) and then stirred at room temperature for 48 h. The resultant mixture was thermally treated at 600 °C for 1 h with a 5 °C/min heating rate and a 30 ml/min nitrogen gas flow. The commercial TiO_2 and TEATFB-doped TiO_2 were termed PT (pristine titania) and DT (doped titania). A size-reduced DT sample was prepared by using paint shaking for 20 min as shown in Fig. 1 and was termed SDT (size-reduced DT).

2.2. Preparation of TiO_2 paste

PT, DT and SDT samples of 2 g each were added to a mixture solution of PEG (poly ethylene glycol, molecular weight: 30,000) solution (0.5 g PEG with 7 ml distilled water), ethanol (Fw: 46.07, 5 ml) and terpienol (Fw: 154.25, 1.5 ml). The resultant mixture was then thermally treated at 100 °C for 6 h.

* Corresponding author. Tel.: +82 42 821 7007; fax: +82 42 822 6637.
E-mail addresses: eujs3915@cnu.ac.kr, youngslee@cnu.ac.kr (Y.-S. Lee).

0925-8388/$ – see front matter © 2011 Elsevier B.V. All rights reserved.
doi:10.1016/j.jallcom.2011.11.011

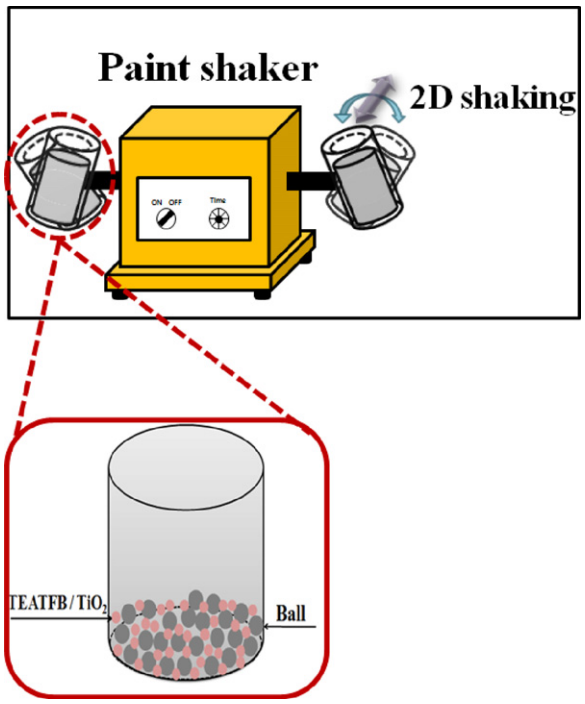

Fig. 1. Diagram of the paint shaker used in this study.

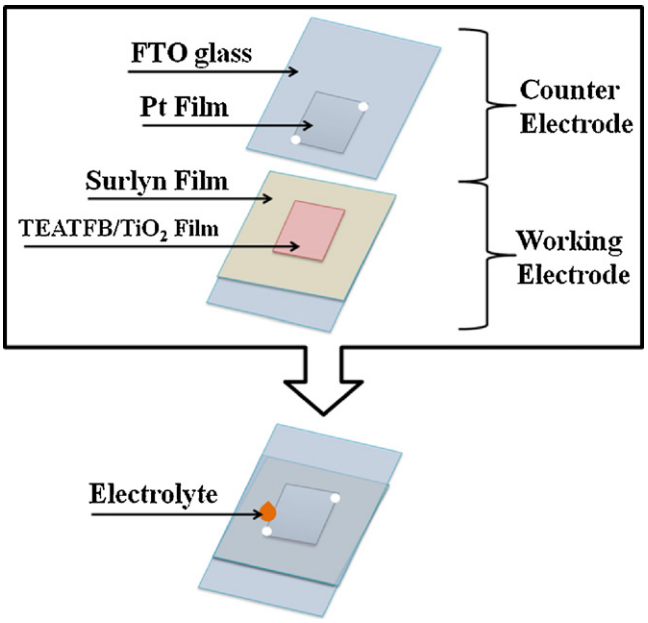

Fig. 2. Diagram for assembly of the DSSC in this study.

2.3. Preparation of working electrode

FTO (fluorine-doped tin oxide, Solaronix) was washed with 2-propanol, ethanol and distilled water several times to remove impurities and was then dried. The prepared TiO_2 paste was loaded by the screen printing method with a V-350 membrane. The TiO_2-paste-loaded FTO was dried at 70 °C for 1 h and then thermally treated at 450 °C for 30 min with a 1.5 °C/min heating rate under an air flow of 30 ml/min. The dye solution was prepared with 25 ml of acetonitrile, 25 ml of r-butyrolactone and 70 mg of dye (Ruthenium535-bis TBA, Solaronix). The prepared TiO_2-paste-loaded FTO was immersed in the prepared dye solution and then stirred at 40 °C for 24 h to absorb the prepared dye in the TiO_2. The thickness of the loaded TiO_2 layer was fixed at 4 μm. The resultant sample was dried at room temperature overnight.

2.4. Preparation of counter electrode

FTO was coated with Pt paste (Pt-1, DYESOL) using a screen printing method and then dried at 70 °C for 3 h. Afterwards, it was thermally treated at 450 °C for 30 min with a 1.5 °C/min heating rate under an air flow of 30 ml/min. The thickness of the loaded Pt layer was fixed at 4 μm.

2.5. Assembly of DSSC

The cell area of the counter and working electrodes was fixed at 1 cm × 1 cm. Two holes in the counter electrode were punched for injection of the electrolyte. A surlyn film (2 cm × 2 cm with a hole of 1 cm × 1 cm, thickness: 25 μm, Solaronix) was located between the counter and working electrodes to bond the two electrodes. They were clipped for immobilization of each part and then thermally treated at 100 °C for 4 min to bond the two electrodes by dissolving the surlyn film. The electrolyte (AN-50, Solaronix) was injected through the holes in the counter electrode. Then, the holes were blocked by surlyn film. The assembly procedure of the cell is presented in Fig. 2.

2.6. Measurement of electrochemical properties

I–V characteristics were measured by a photocurrent–voltage (*I–V*) curve analyzer (IVIUM Technologies, PECK2400-N, version 2.1) under AM 1.5 (100 mW/cm^2) irradiation using a solar simulator (Peccell Technologies, PEC-L01). Electrochemical impedance spectroscopy (EIS) measurements were carried out under open circuit with an electrochemical work station (ZAHNER, IM6ex) with a frequency range of 10 mHz to 100 kHz. The magnitude of the alternating signal was 5 mV. Impedance measurements were carried out under a forward bias of 600 mV.

Intensity-modulated photocurrent spectroscopy (IMPS) under short-circuit conditions and intensity-modulated photovoltage spectroscopy (IMVS) under open-circuit conditions were performed on the DSSCs. A light emitting diode (LED, 635 nm) was used as the light source. The light intensity was modulated with a sine-shaped voltage supplied by a Solartron 1255B frequency response analyzer (FRA) over the appropriate frequency range. The DC light generated by the LED, with the intensity up to 2 W m^{-2}, was used as the superimposed constant illumination in the measurements. The amplitude and phase shift of the current response with respect to the modulation of the light intensity were measured with FRA.

2.7. Characterization of samples

The surface morphology of the samples was investigated by using a field emission scanning electron microscope (FE-SEM, Hitachi, S-5500). Images were taken without prior treatment (e.g., Pt coating) to ensure the acquisition of accurate images. The average size of the clusters was measured by the software program installed on the FE-SEM apparatus. The particle size density was evaluated using a laser scattering particle size analyzer (HELOS/RODOS & SUCELL, Sympatec GmbH Co., Germany) to investigate the size reduction effect caused by the paint shaker. The XPS spectra of used samples in this study were obtained with a MultiLab 2000 spectrometer (Thermo Electron Co., England) to evaluate the chemical species on the surface of TiO_2 based on effects of multi-element doping. Al Kα (1485.6 eV) X-rays were used with a 14.9-keV anode voltage, a 4.6-A filament current and a 20-mA emission current. All samples were treated at 10^{-9} mbar to remove impurities. The survey spectra were obtained with a 50-eV pass energy and a 0.5-eV step size. Core level spectra were obtained at 20-eV pass energy with 0.05-eV step size.

3. Results

3.1. Surface morphology of prepared samples

FE-SEM images of the PT, DT and SDT samples are presented in Fig. 3, displaying the surface morphology. The working electrodes after loading three samples are presented in Fig. 3(a), (c) and (e). And the morphologies of prepared three samples are in Fig. 3(b), (d) and (f). The agglomeration degree of TiO_2 was significantly decreased via using a paint shaker as seen in Fig. 3(e). The average particle size of PT, as measured by the software program installed on the FE-SEM apparatus, is about 27.2 ± 6.2 nm. The particle size became slightly larger due to B, C, N and F doping effects on the surface of TiO_2. The effect of the size reduction of TiO_2 is shown in the SDT sample, with an average particle size of 22.3 ± 4.5 nm. This result correlates well with the result of the particle size distribution shown in Fig. 4. The peak position was shifted to left side significantly indicating the size reduction of TiO_2. Therefore, it can be concluded that the contact area of TiO_2 with the dye or the electrolyte may be significantly increased, leading to an enhanced reaction at the TiO_2/dye/electrolyte interface for high efficiency of the DSSC because the high contact area between semiconductor

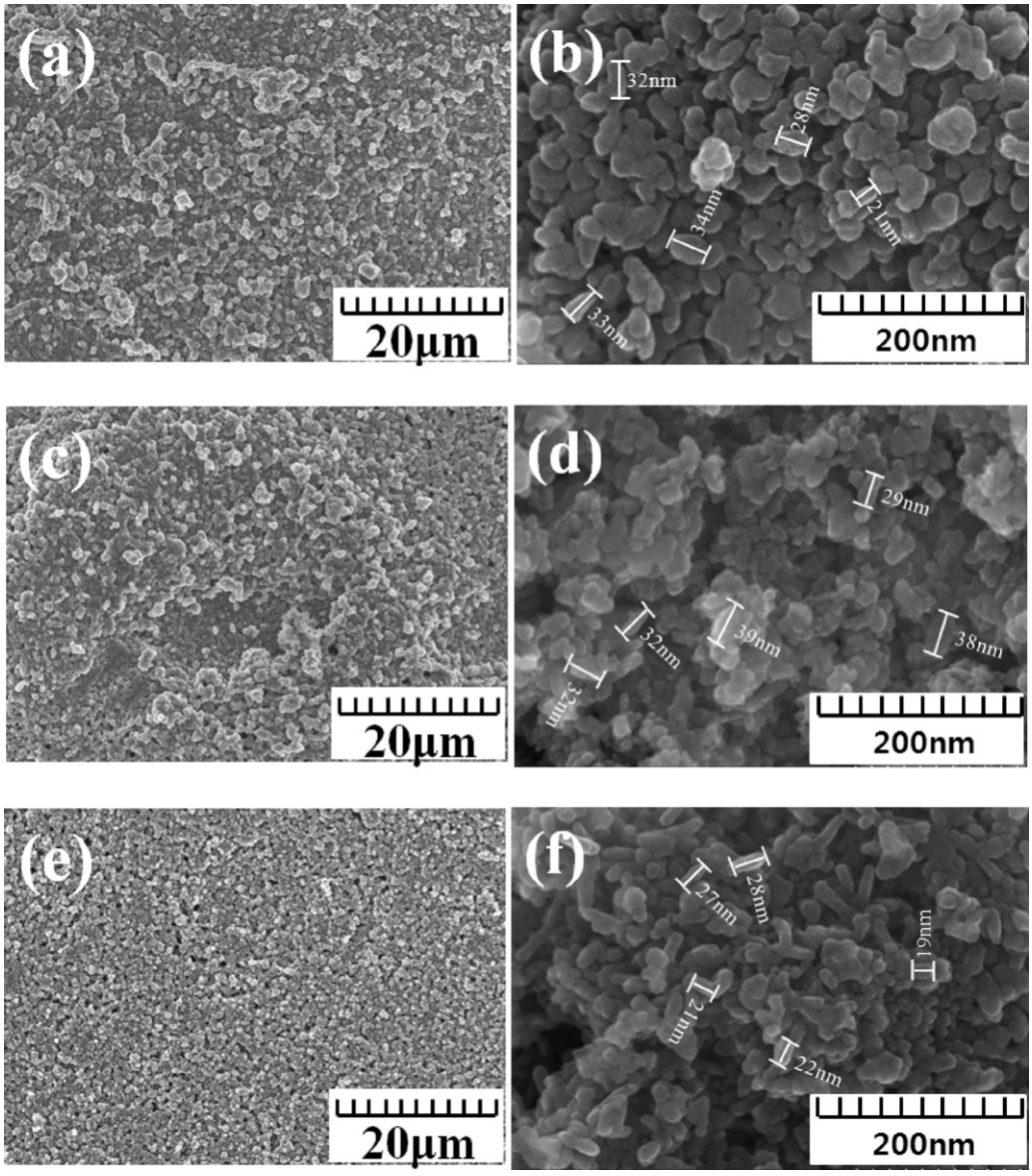

Fig. 3. FE-SEM images of (a and b) PT, (c and d) DT and (e and f) SDT.

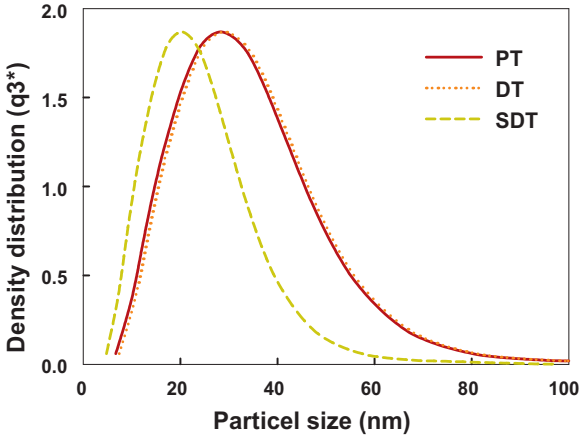

Fig. 4. Particle size density distribution of PT, DT and SDT samples.

and dye can provide more enough sites for an efficient electron transfer from dye to TiO_2.

3.2. Chemical analysis of B, C, N and F dopants on the surface of TiO_2

The chemical bonds of B, C, N and F with TiO_2 were determined by XPS analysis as shown in Fig. 5. Fig. 5(a) shows the F 1s XPS spectrum. The main peak of the asymmetrical line shape in this spectrum can be assigned to structures containing oxyfluoride (F–Ti–O) functional groups, whereas the shoulder at 689 eV is related to the F–Ti bond [10]. These findings reveal that fluorine is incorporated into the TiO_2 by replacing oxygen atoms in its lattice, forming non-stoichiometric $TiO_{2-x}F_x$ structures [11]. The formation of these $TiO_{2-x}F_x$ structures, in which the fluorine ions are incorporated in the TiO_2 lattice, contributes to the improved TiO_2 crystallinity [12]. As shown in Fig. 5(b), the N 1s peak at 400 eV was observed in the doped TiO_2 samples. Similarly, a significant peak near 402 eV and a minor peak near 400 eV, assigned to the N 1s peak, have been reported in N-doped TiO_2 [13]. Sakthivel and Kisch [10] prepared nitrogen-doped titania from titanium tetraisopropoxide

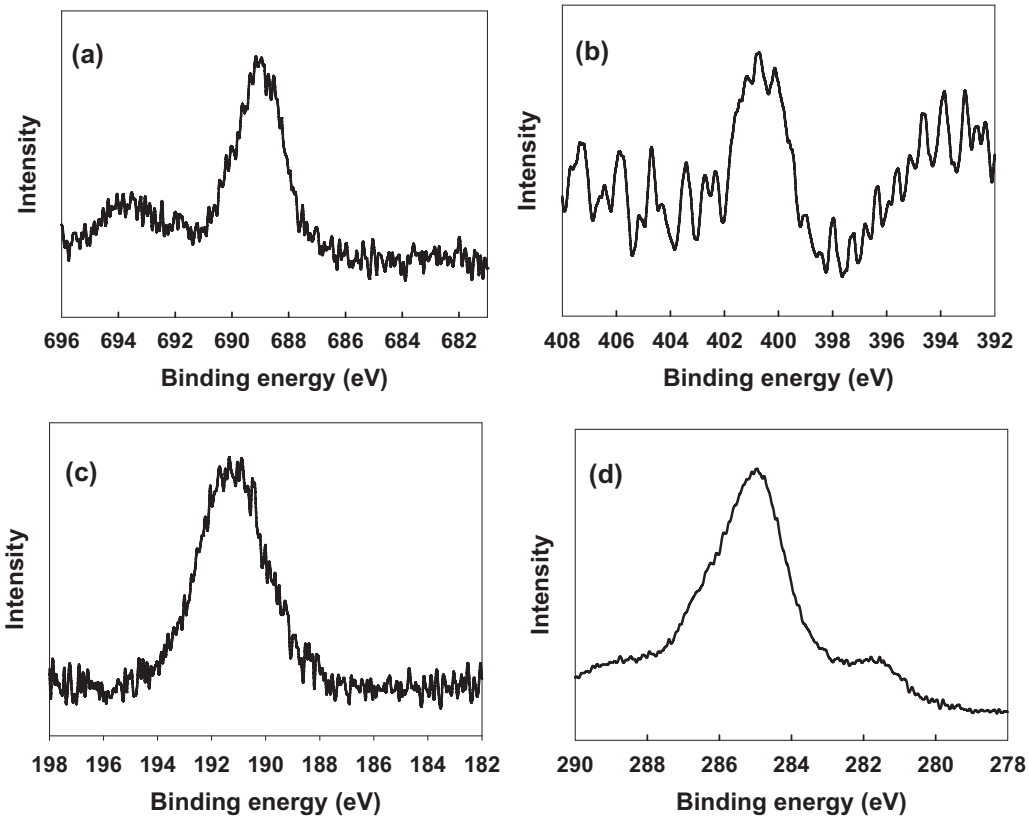

Fig. 5. XPS peaks of SDT: (a) F 1s, (b) N 1s, (c) B 1s and (d) C 1s.

or titanium tetrachloride and thiourea [14]. They observed a binding energy of 400.1 eV, assigned to hyponitrite at the surface, which was attributed to the doped nitrogen. Fig. 5(c) shows the XPS spectrum of the B 1s region on the surface of the SDT sample. Note that the B 1s region contains only one peak and that the binding energy shifts from 191.1 eV to 191.5 eV. This shift implies the formation of a weak Ti–B bond and is also attributed to the interference effects of other elements bonding with Ti. By taking into account the standard binding energy of B 1s in TiB_2 (187.5 eV, B–Ti bond), this result indicates that the boron atom is probably incorporated with the TiO_2 to some extent and that the chemical environment surrounding the boron is similar to that of the TiB_2 [15]. In Fig. 5(d), the peaks near 285 eV are attributed to C 1s [16]. In the case of C and F, there is no observable peak shift, which is due to the strong bond between the F and C atoms and the Ti particles. In the SDT sample, the elemental compositions of O, Ti, N, C, F and B were 57.6, 24.5, 0.9, 14.2, 1.5 and 1.3 at.%. Resultantly, $TiO_{2-x}N_x$ ($x = 0.015$), $TiO_{2-x}C_x$ ($x = 0.197$), $TiO_{2-x}B_x$ ($x = 0.022$) and $TiO_{2-x}F_x$ ($x = 0.025$) structures were obtained in this study.

3.3. Photocurrent–voltage behavior of DSSCs

The photocurrent–voltage curves of the DSSCs are presented in Fig. 6. The open-circuit voltage (V_{oc}) and short-circuit current (I_{sc}) of each sample were measured at $I = 0$ mA and $V = 0$ V. The maximum voltage (V_{max}) and maximum current (I_{max}) were calculated at the point of maximum power (P_{max}, assigned as point a, b or c in Fig. 6) based on following equation [17–19]:

$$P = I \times V \tag{1}$$

Furthermore, the fill factor (FF) and efficiency (η) are given by

$$\mathrm{FF} = \frac{V_{max} \times I_{max}}{V_{oc} \times I_{sc}} \tag{2}$$

$$\eta(\%) = \left[\frac{V_{oc} \times I_{sc} \times \mathrm{FF}}{P_{in} \times S}\right] \times 100 \tag{3}$$

In Eq. (3), S and P_{in} represent the area of the thin film on the working electrode (1 cm^2) and the incident light power (100 mW/cm^2), respectively. The measured factors are presented in Table 1. I_{sc} increased by a factor greater than two based on the effects of doping elements and size reduction in DT and SDT, respectively. When comparing the values of I_{sc} and I_{max} in each sample, I_{max} showed a slightly smaller current, indicating a small shunt resistance (R_{SH}) in the DSSC [20]. However, the gap of V_{oc} and V_{max} (ΔV) in each sample showed a higher change ratio; the values of $\Delta V/V_{oc}$ of PT, DT and SDT were 29.7, 22.9 and 18.4%, respectively. This trend is

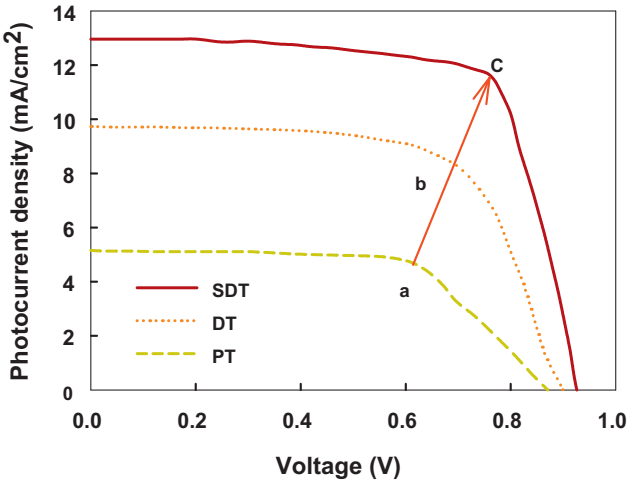

Fig. 6. *I–V* characteristics of the DSSC with PT, DT and SDT.

Table 1
Photovoltaic parameters of DSSC.

	V_{oc} (V)	I_{sc} (mA cm^{-2})	V_{max} (V)	I_{max} (mA cm^{-2})	FF (%)	ΔV^a (V)	η (%)
SDT	0.925	12.959	0.755	11.697	73.673	0.170	8.831
DT	0.897	9.737	0.692	8.360	66.236	0.205	5.785
PT	0.865	5.156	0.608	4.730	64.482	0.257	2.876

[a] ΔV: $V_{oc} - V_{max}$.

attributed to a decreased series resistance (R_S), and it is beneficial for the higher FF and working voltage in DSSCs [21–23]. The FF also increased dramatically, from 64.5 to 73.7%, based on the effects of the multi-element doping of B, C, N and F and the size reduction of the TiO_2 particles. The efficiency of the DSSC was improved over three times, up to 8.8%.

4. Discussion

4.1. Suggested mechanism of improved efficiency of prepared DSSCs

The suggested mechanism of the DSSC is depicted based on the effects of B, C, N and F doping and the size reduction of TiO_2. In Fig. 7(a), the DSSC mechanism for PT is presented. The electrons are excited by solar energy from the HOMO to the LUMO in dye molecule, indicated as ①. These excited electrons diffuse into the conduction band (CB) of TiO_2, indicated as ②. Then, the electrons travel through the CB of the TiO_2 layer towards the FTO of the working electrode, indicated as ③. In this process, a large number of electrons move to the LUMO of the dye or electrolyte due to electron trapping effects. This process results in electron recombination, which is indicated as ④. The reason is considered that the electron transfer time is a few nanoseconds from the LUMO of the dye to the CB of TiO_2, whereas the electron transfer time in the CB of TiO_2 is a few milliseconds [24,25]. Thus, the original voltage intensity (indicated as ⑤) drops significantly, shown as ⑥. Eventually, the working voltage intensity is determined as ⑦ [26–28].

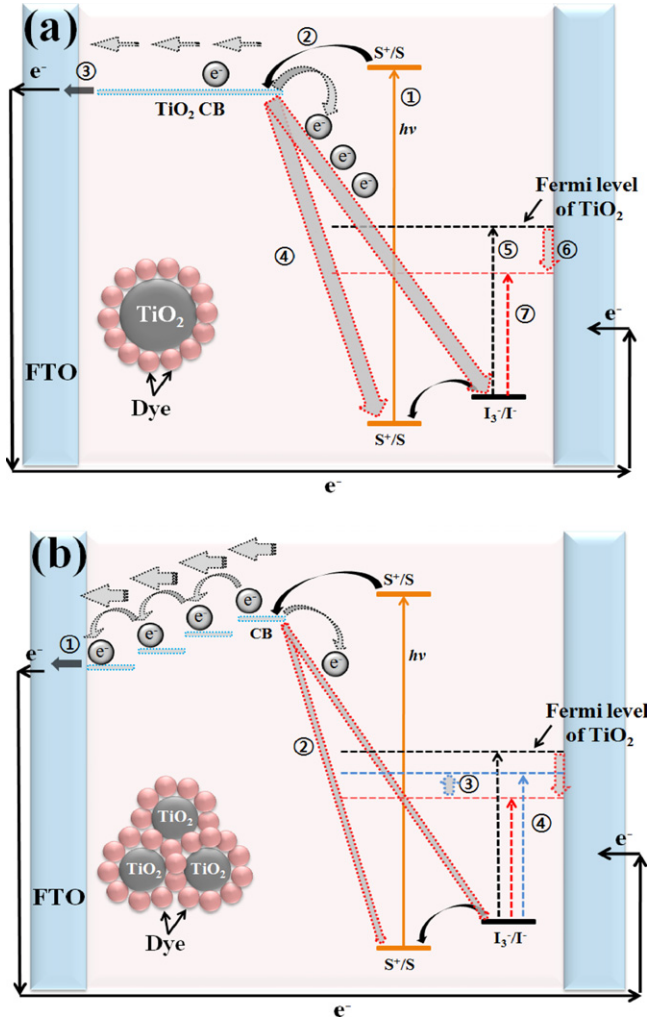

Fig. 7. Suggested mechanism for the improved efficiency of the DSSC based on inorganic element doping and the size reduction of TiO_2 with (a) PT (suggested by Grätzel [24]) and (b) SDT.

The mechanism for preventing a voltage drop is shown in Fig. 7(b). The electrons moving to the dye or electrolyte can be transferred through CB of TiO_2 based on effects of multi-element dopants. It is well known that each B [29], C [30], N [31] and F [32] dopant lower the CB of TiO_2 resulting the steps with different energy level as shown in ① [33–35]. These multi-energy level steps can accelerate the electron flow for lower energy lever resulting in an electron path valley. When comparing with PT sample shown in Fig. 7(a), it can be estimated that the long electron path way in the CB of TiO_2 with same energy level is not efficient for electron transfer. Even though a little voltage drop can be estimated by the lowered CB of TiO_2, it seems that the preventing effect of electron recombination is much powerful. Eventually, the enlarged electron path way can be constructed leading the efficient electron transfer from dye to FTO working electrode through CB of TiO_2 as shown in ① and ②. In this process, the enlarged contact area between the semiconductor and the dye or electrolyte might also improve the electron charge transfer at the interface [36,37]. These electrons go to the FTO of the working electrode, resulting in enhanced voltage intensity, which is indicated as ③. Thus, an improved voltage intensity can be obtained, which is indicated as ④. These results are correlated with the increased V_{max} and decreased ΔV shown in Table 1 and Fig. 6. In conclusion, a drop in the voltage intensity is prevented by electron recombination and significantly improves the efficiency of the DSSC.

4.2. EIS of samples

The EIS results of PT, DT and SDT are presented by Nyquist plots in Fig. 8. In general, the impedance spectrum of the DSSC shows three semicircles in the frequency range of 10 mHz to 100 kHz. The first semicircle is related to the charge transfer at the counter electrode measured in the kHz range. The second semicircle is related to the electron transport at the TiO_2/dye/electrolyte interface in the range of 1–100 Hz. The third semicircle shows the Warburg diffusion process of I^-/I_3^- in the electrolyte, measured in the mHz range [38–40]. These three semicircles indicate the R_{ct1}, R_{ct2} and R_{diff} of an equivalent circuit, as shown in Fig. 8(c). In this study, each curve showed only two semicircles. The R_{diff} was not obvious, and it was overlapped by R_{ct2} due to the very thin spacer used in the devices. This result also agrees with the results of another group [41]. In addition, the electrolyte is not an important parameter because we used the same electrolyte in prepared DSSCs. Thus, the third semicircle was not considered in this paper. The second semicircle decreased significantly due to the effects of the doping of B, C, N

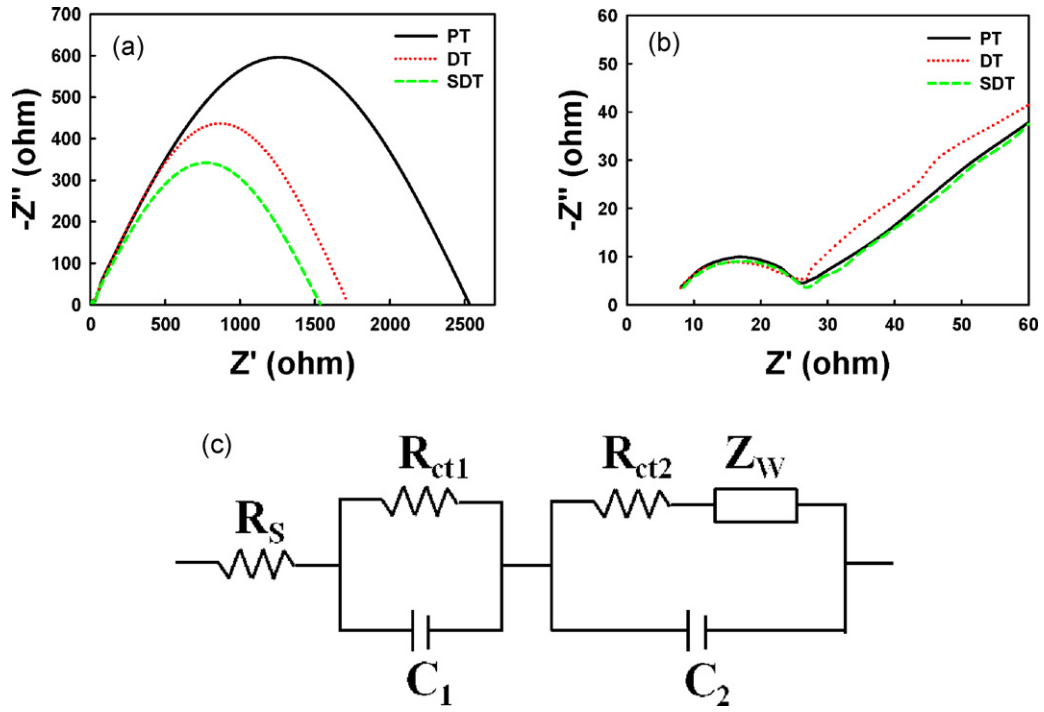

Fig. 8. Nyquist plots of PT, DT and SDT samples measured by EIS as measured in (a) 1-kHz and (b) kHz range and (c) the equivalent circuit used to represent the interface in composite solar cells.

and F inorganic elements and the size reduction of TiO_2, as shown in Fig. 8(a). It is notable that the electron flow from the LUMO of the dye to the FTO through the CB of TiO_2 became more efficient, supporting the mechanism illustrated in Fig. 7. In the case of the first semicircle, shown in Fig. 8(b), three samples showed the similar values because the preparation condition of counter electrode was same. And the R_s related to the sheet resistance of the FTO did not show any significant change because the same FTO glasses were used in all samples. Therefore, it is notable that the electron charge transfer improved at the semiconductor/dye/electrolyte interface due to the effects of B, C, N and F dopants and the size reduction of TiO_2.

4.3. IMPS and IMVS of samples

IMPS and IMVS were conventional methods to investigate the electron transfer and recombination process. The response plots of IMPS and IMVS were shown in Fig. 9. The electron transport time (τ_t) and the electron recombination time (τ_r) can be estimated by from the IMPS and IMVS plots by following Eqs. (4) and (5) [42,43]:

$$\tau_t = 0.5 \times \pi \times f^1_{min} \quad (4)$$

$$\tau_r = 0.5 \times \pi \times f^2_{min} \quad (5)$$

where f^1_{min} and f^2_{min} are the characteristic frequency at the minimum of the imaginary IMPS and IMVS, respectively. In addition, the electron diffusion coefficient (D_n) and the electron diffusion length (L_n) can be determined on the basis of film thickness (d, 4 μm in this study), τ_t and τ_r by following Eqs. (6) and (7) [42–44]:

$$D_n = \frac{d^2}{2.35 \times \tau_t} \quad (6)$$

$$L_n = (D_n \times \tau_r)^{0.5} \quad (7)$$

The calculated results are presented in Table 2. It was confirmed that electron was transported more quickly through TiO_2 working electrode and electron recombination was retarded significantly.

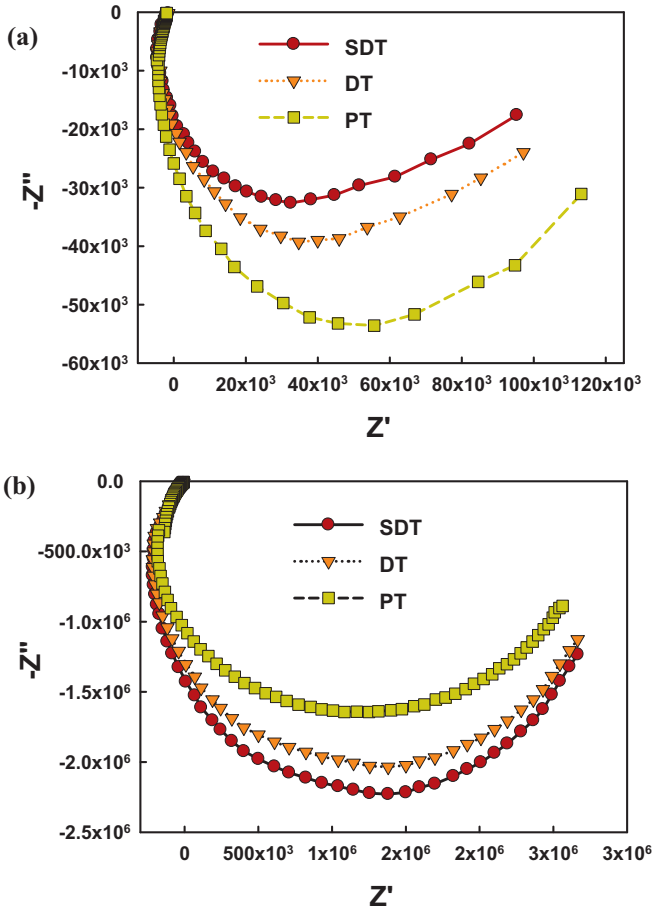

Fig. 9. IMPS (a) and IMVS (b) of samples.

Table 2
IMVS and IMPS parameters.

	PT	DT	SDT
f^1_{min} (Hz)	1786	2831	3177
f^2_{min} (Hz)	5.639	4.479	3.992
τ_t (s)	8.9×10^{-5}	5.6×10^{-5}	5.1×10^{-5}
τ_r (s)	2.8×10^{-2}	3.6×10^{-2}	4.0×10^{-2}
D_n (cm^2/s)	0.7×10^{-3}	1.2×10^{-3}	1.4×10^{-3}
L_n (μm)	46.4	65.6	73.6

Accordingly, L_n increased about 1.6 times and D_n improved about 2-folds when comparing PT and SDT samples based on effects of multi-element doping and size reduction of TiO_2. These results surely support the suggested mechanism explained in Section 4.1 as an evidence.

5. Conclusions

B, C, N and F doped TiO_2 was prepared as a semiconductor in the working electrode of a DSSC. The fill factor and efficiency of the DSSC improved by around 14% and by more than a factor of 3, respectively, based on the effects of multi-element dopants and the size reduction of TiO_2. The mechanism for the high efficiency of the DSSC was suggested by EIS analysis. The B, C, N and F dopants seem to prevent the electrons in the CB of TiO_2 from returning to the dye or electrolyte for recombination due to the efficient electron transfer in TiO_2 working electrode. In addition, the size of TiO_2 was reduced by using a paint shaker, which was beneficial for active reactions at the TiO_2/dye/electrolyte interface due to the enlarged contact area. In conclusion, high efficiency of a DSSC was obtained based on the effects of inorganic element dopants and size reduction of TiO_2.

References

[1] A. Qurashi, M.F. Hossain, M. Faiz, N. Tabet, M.W. Alam, N.K. Reddy, J. Alloys Compd. 503 (2010) L40–L43.
[2] J. Mou, W. Zhang, J. Fan, H. Deng, W. Chen, J. Alloys Compd. 509 (2011) 961–965.
[3] J. Zhang, W. Que, Q. Jia, P. Zhong, Y. Liao, X. Ye, Y. Ding, J. Alloys Compd. 509 (2011) 7421–7426.
[4] Y.S. Jung, A.R. Sathiya Priya, M.K. Lim, S.Y. Lee, K.J. Kim, J. Photochem. Photobiol. A-Chem. 209 (2010) 174–180.
[5] K.L. McCall, J.R. Jennings, H. Wang, A. Morandeira, L.M. Peter, J.R. Durrant, L.J. Yellowlees, J.D. Woollins, N. Robertson, J. Photochem. Photobiol. A-Chem. 202 (2009) 196–204.
[6] S.Y. Cha, Y.G. Lee, M.S. Kang, Y.S. Kang, J. Photochem. Photobiol. A-Chem. 211 (2010) 193–196.
[7] S. Yang, H. Kou, H. Wang, K. Cheng, J. Wang, Electrochim. Acta 55 (2009) 305–310.
[8] Y. Lee, M. Kang, Mater. Chem. Phys. 122 (2010) 284–289.
[9] C.S. Chou, R.Y. Yang, C.K. Yeh, Y.J. Lin, Powder Technol. 194 (2009) 95–105.
[10] S. Sakthivel, H. Kisch, Chem. Phys. Chem. 4 (2003) 487–490.
[11] R. Swanepoel, J. Phys. E: Sci. Instrum. 16 (1983) 1214–1222.
[12] T. Giannakopoulou, N. Todorova, C. Trapalis, T. Vaimakis, Mater. Lett. 61 (2007) 4474–4477.
[13] W. Zhao, W. Ma, C. Chen, J. Zhao, Z. Shuai, J. Am. Chem. Soc. 126 (2004) 4782–4783.
[14] C. Chen, H. Bai, S. Chang, C. Chang, W. Den, J. Nanopart. Res. 9 (2006) 365–375.
[15] D. Chen, D. Yang, Q. Wang, Z. Jiang, Ind. Eng. Chem. Res. 45 (2006) 4110–4116.
[16] J.S. Im, I.J. Park, S.J. In, T. Kim, Y.S. Lee, J. Fluor. Chem. 130 (2009) 1111–1116.
[17] Y. Lee, J. Chae, M. Kang, J. Ind. Eng. Chem. 16 (2010) 609–614.
[18] J. Wu, G. Xie, J. Lin, Z. Lan, M. Huang, Y. Huang, J. Power Sources 195 (2010) 6937–6940.
[19] Z. Tang, J. Wu, Q. Li, Z. Lan, L. Fan, J. Lin, M. Huang, Electrochim. Acta 55 (2010) 4883–4888.
[20] H. Chen, A.D. Pasquier, G. Saraf, J. Zhong, Y. Lu, Semicond. Sci. Technol. 23 (2008) 045004.
[21] K. Li, Y. Luo, Z. Yu, M. Deng, D. Li, Q. Meng, Electrochem. Commun. 11 (2009) 1346–1349.
[22] S. Gagliardi, L. Giorgi, R. Giorgi, N. Lisi, T.D. Makris, E. Salernitano, A. Rufoloni, Superlattices Microstruct. 46 (2009) 205–208.
[23] Q. Qin, J. Tao, Y. Yang, Synth. Met. 160 (2010) 1167–1172.
[24] A. Kay, M. Grätzel, Chem. Mater. 14 (2002) 2930–2935.
[25] S.S. Kim, J.H. Yum, Y.E. Sung, Sol. Energy Mater. Sol. Cells 79 (2003) 495–505.
[26] L. Dupuy, S. Haller, J. Rousset, F. Donsanti, J.F. Guillemoles, D. Lincot, F. Decker, Electrochem. Commun. 12 (2010) 697–699.
[27] L. Lu, R. Li, K. Fan, T. Peng, Sol. Energy 84 (2010) 844–853.
[28] P. Balraju, P. Suresh, M. Kumar, M.S. Roy, G.D. Sharma, J. Photochem. Photobiol. A-Chem. 206 (2009) 53–63.
[29] H. Tian, L. Hu, C. Zhang, S. Chen, J. Sheng, L. Mo, W. Liu, S. Dai, J. Mater. Chem. 21 (2011) 863–868.
[30] I. Hiroshi, W. Seitaro, H. Kazuhito, Thin Solid Films 510 (2006) 21–25.
[31] S.H. Kang, H.S. Kim, J.Y. Kim, Y.E. Sung, Mater. Chem. Phys. 124 (2010) 422–426.
[32] Y. Wu, M. Xing, B. Tian, J. Zhang, F. Chen, Chem. Eng. J. 162 (2010) 710–717.
[33] J.S. Im, S.M. Yun, Y.S. Lee, J. Colloid Interface Sci. 336 (2009) 183–188.
[34] J.S. Im, M.J. Jung, Y.S. Lee, J. Colloid Interface Sci. 339 (2009) 31–35.
[35] J.S. Im, J.G. Kim, S.H. Lee, Y.S. Lee, Colloid Surf. A-Physicochem. Eng. Aspects 20 (2010) 151–157.
[36] G.W. Lee, S.Y. Bang, C. Lee, W.M. Kim, D. Kim, K. Kim, N.G. Park, Curr. Appl. Phys. 9 (2009) 900–906.
[37] M.H. Seo, M. Yuasa, T. Kida, J.S. Huh, N. Yamazoe, K. Shimanoe, Sens. Actuator B-Chem. 154 (2011) 251–256.
[38] K. Pan, Y. Dong, C. Tian, W. Zhou, G. Tian, B. Zhao, H. Fu, Electrochim. Acta 54 (2009) 7350–7356.
[39] L. Bay, K. West, B. Winther-Jensen, T. Jacobsen, Sol. Energy Mater. Sol. Cells 90 (2006) 341–351.
[40] J.A. Mikroyannidis, M.M. Stylianakis, M.S. Roy, P. Suresh, G.D. Sharma, J. Power Sources 194 (2009) 1171–1179.
[41] L.Y. Lin, C.P. Lee, R. Vittal, K.C. Ho, J. Power Sources 195 (2010) 4344–4349.
[42] B.H. Lee, M.Y. Song, S.Y. Jang, S.M. Jo, S.Y. Kwak, D.Y. Kim, J. Phys. Chem. C 113 (2009) 21453–21457.
[43] P.S. Archana, R. Jose, C. Vijila, S. Ramakrishna, J. Phys. Chem. C 113 (2009) 21538–21542.
[44] D. Zhang, T. Yoshida, T. Oekermann, K. Furuta, H. Minoura, Adv. Funct. Mater. 16 (2006) 1228–1234.